Calculation of the QCD phase diagram at finite temperature, and baryon and isospin chemical potentials

A. Barducci,* R. Casalbuoni,† G. Pettini,‡ and L. Ravagli§
Department of Physics, University of Florence and INFN Sezione di Firenze, Via G. Sansone 1, I-50109, Sesto F.no, Firenze, Italy
(Received 12 February 2004; published 27 May 2004)

We study the phases of a two-flavor Nambu–Jona-Lasinio model at finite temperature T, and baryon and isospin chemical potentials $\mu_B=(\mu_u+\mu_d)/2$, $\mu_I=(\mu_u-\mu_d)/2$. This study completes a previous analysis where only small isospin chemical potentials μ_I were considered.

DOI: 10.1103/PhysRevD.69.096004 PACS number(s): 11.10.Wx, 12.38.−t, 25.75.Nq

I. INTRODUCTION

The possible formation of a pion condensate due to a finite isospin chemical potential μ_I has been, in recent years, the subject of several papers [1–14]. Consequently, the reconstruction of the QCD phase diagram at finite temperature and quark densities, such as those attainable in Earth experiments and in the interior of stars, is even more challenging due to the addition of μ_I, in addition to temperature T and baryon chemical potential μ_B. Various regions of the phase diagram correspond to different experimental settings. Actually, the behavior of QCD at high temperature and low baryon densities is central to the relativistic heavy-ion collisions: experiments at CERN and BNL Relativistic Heavy Ion Collider (RHIC) are expected to produce hadronic matter in this regime. On the other hand, the description of neutron star interiors requires the knowledge of cold nuclear matter at large baryon densities. However, nature also provides us with systems at finite isospin chemical potential μ_I in the form of asymmetric-isospin matter inside neutron stars: nuclear matter has a finite (negative) isospin I_3 density due to Coulomb interactions, apart from finite baryon-number density. Moreover, in any realistic experimental setting in relativistic heavy-ion collisions there is a nonzero, even if small, μ_I.

Our present description of the QCD phase diagram in the plane (μ_B, T) anticipates the existence of a tricritical point separating first-order transitions in the regions of low temperatures from crossover transitions in the low baryon chemical potential and high-temperature regime [15–21]. In recent years various other nontrivial phases of QCD at low temperatures and high baryon chemical potentials have been discovered, such as the color flavor locking (CFL) phase and the two-color superconducting (2SC) phase (for a review, see, Ref. [22]).

Coming back to the effects of the isospin chemical potential μ_I, pion condensation has so far been primarily investigated by means of low-energy models based on chiral Lagrangians [5,7,8,23]. Although these models are well suited to study the phases of QCD as they have the right symmetry properties, they do not include the combined effects of the isospin chemical potential μ_I with a finite baryon chemical potential μ_B in order to study the pattern of chiral symmetry breaking and restoration as well. To consider both μ_B and μ_I, we need a model with quarks as microscopic degrees of freedom. The effect of small μ_I (up to half of the pion mass) has been investigated in Ref. [12] in the context of the Nambu–Jona-Lasinio model and in *ladder* QCD [14]. The result is the splitting of the critical curves for chiral symmetry restoration for the two light flavors, whereas a full study for arbitrary μ_I has only been done in the context of a random matrix model [11].

Studies on the lattice have been performed at finite μ_I and $\mu_B=0$ in Refs. [24–28] and with a finite μ_B and $\mu_I=0$ in Refs. [28–32]. In a recent work [33] the effect of both μ_B and a small μ_I has also been considered. The case of high μ_B and small μ_I has been considered in Ref. [34].

In this work we extend the analysis of Refs. [12,14] where it was found that the first-order transition line ending at the tricritical point of the case $\mu_I=0$ actually splits into two first-order transition lines and correspondingly two crossover regions are present at low values of baryon chemical potential. In particular we will be working in the context of a NJL model with a form factor included such as to imply a decreasing of the fermion self-energy compatible with the operator product expansion.

It should also be noticed that in Ref. [13] the NJL model has been augmented by the four-fermi instanton interaction relevant in the case of two flavors. These authors have found that the coupling induced by the instanton interaction between the two flavors might completely wash the splitting of the first-order transition line. This happens for values of the ratio of the instanton coupling to the NJL coupling of order 0.1–0.15.

In Sec. II we summarize the relevant features of the NJL model we have considered, with isospin charge included. The one-loop effective potential and the values of the fit parameters are included. In Sec. III we discuss the various equilibrium phases of the model, together with the corresponding symmetries, by studying the behavior of the scalar and pion condensates with respect to different thermodynamical parameters among T, μ_B, μ_I (or μ_u, μ_d). Results are shown for growing temperatures, starting from zero up to

*Electronic address: barducci@fi.infn.it
†Electronic address: casalbuoni@fi.infn.it
‡Electronic address: pettini@fi.infn.it
§Electronic address: ravagli@fi.infn.it

temperatures above that of the critical ending point. Finally, Sec. IV is devoted to conclusions.

II. MODEL

Our purpose is to explore the structure of the phase diagram for chiral symmetry and pion condensation in QCD at finite temperature and quark densities, by using a microscopic model with quark degrees of freedom. This task has been accomplished, up to now, in the context of a random matrix model simulating QCD with two flavors [11] and, in the case of small differences between the u and d quark chemical potentials, also in the Nambu–Jona-Lasinio model (NJL) [12] and in *ladder* QCD [14].

One reason for using a model with quarks as microscopic degrees of freedom is that it gives us the possibility of studying chiral symmetry breaking and pion condensation at both finite isospin and baryon chemical potentials, which is not possible within effective chiral models.

In Ref. [12], the authors made use of the NJL model with a suitable form factor included in the quark self-energy to mimic asymptotic freedom [21,35]. This version of the NJL model turns out to be very close to *ladder* QCD as developed in Refs. [16,36] where the momentum dependence of the quark self-energy is consistently dictated by the study of the Schwinger-Dyson equation within a variational approach (see the previous references for details). However, although *ladder* QCD is a covariant and self-consistent approach, the dependence on the four-momentum of the quark self-energy makes the numerical computation of the one-loop effective potential with finite quark densities much more onerous with respect to the NJL case, where the quark self-energies depend only on the three-momentum. For this reason, in the present work we study the NJL model. It is reasonable to expect that when employing *ladder* QCD, the resulting physical picture does not considerably differ from that of the NJL model. This has been the case in previous applications too [16,17,19].

As already said in the Introduction we are not going to consider the effects of di-fermion condensation. Therefore our results can be considered valid only outside the region of the color superconductive phase, which is roughly in the region defined by $\mu_B \gtrsim 400$–500 MeV and $T \lesssim 50$ MeV. At the same time we will not consider regions at values of μ_u or μ_d higher than 400–500 MeV where other difermion condensates might arise (see for instance Ref. [37]).

Let us now consider the Lagrangian of the NJL model with two flavors u,d with the same mass m but different chemical potentials μ_u and μ_d,

$$\begin{aligned}\mathcal{L} &= \mathcal{L}_0 + \mathcal{L}_m + \mathcal{L}_\mu + \mathcal{L}_{int} \\ &= \bar{\Psi} i \hat{\partial} \Psi - m \bar{\Psi} \Psi + \Psi^\dagger A \Psi \\ &\quad + G \sum_{a=0}^{3} [(\bar{\Psi} \tau_a \Psi)^2 + (\bar{\Psi} i \gamma_5 \tau_a \Psi)^2], \end{aligned} \tag{1}$$

where

$$\Psi = \begin{pmatrix} u \\ d \end{pmatrix}, \quad A = \begin{pmatrix} \mu_u & 0 \\ 0 & \mu_d \end{pmatrix}$$

is the matrix of chemical potentials and τ_a, $a=0,1,2,3$, is the set of the three Pauli matrices plus the identity.

We note that we can express $\mathcal{L}_\mu$ either by using the variables μ_u, μ_d or the two combinations $\mu_B = (\mu_u + \mu_d)/2$ and $\mu_I = (\mu_u - \mu_d)/2$, which couple to the baryon charge density and to the third component of isospin, respectively,

$$\mathcal{L}_\mu = \mu_B \Psi^\dagger \Psi + \mu_I \Psi^\dagger \tau_3 \Psi. \tag{2}$$

To study whether a pion condensate shows up, we need to calculate the effective potential. This is obtained by using the standard technique to introduce Bosonic (collective) variables through the Hubbard-Stratonovich transformation and by integrating out the fermion fields in the generating functional. However, the effective potential that we have considered is not directly obtained from the Lagrangian in Eq. (1). To mimic asymptotic freedom we want to include a form factor as in Ref. [35] and we thus follow the same procedure as in Refs. [12,21]. The result is a one-loop effective potential which generalizes that of the theory described by the Lagrangian in Eq. (1), and which reduces to it in the limit of a constant form factor $F(\vec{p}) = 1$,

$$V = \frac{\Lambda^2}{8G} (\chi_u^2 + \chi_d^2 + 2\rho^2) + V_{\log}, \tag{3}$$

$$V_{\log} = -\,\mathrm{Tr} \log \begin{pmatrix} h_u & -F^2(\vec{p}) \Lambda \rho \gamma_5 \\ F^2(\vec{p}) \Lambda \rho \gamma_5 & h_d \end{pmatrix},$$

$$h_f = (i\omega_n + \mu_f)\gamma_0 - \vec{p} \cdot \vec{\gamma} - [m + F^2(\vec{p}) \Lambda \chi_f], \tag{4}$$

where ω_n are the Matsubara frequencies and the dimensionless fields χ_f and ρ are connected to the condensates by the following relations:

$$\chi_f = -4G \frac{\langle \bar{\Psi}_f \Psi_f \rangle}{\Lambda},$$

$$\rho = -2G \frac{\langle \bar{u} \gamma_5 d - \bar{d} \gamma_5 u \rangle}{\Lambda} \tag{5}$$

and are variationally determined at the absolute minimum of the effective potential. In the previous equations, Λ is a mass scale appearing in the form factor $F(\mathbf{p}^2) = \Lambda^2/(\Lambda^2 + \mathbf{p}^2)$ [35]. It is worth noting that the one-loop effective potential in Eq. (4) has the same expression as the one derived in Ref. [14] within *ladder* QCD. Therein, multiplying the scalar and pseudoscalar fields, there was a test function guessed from the study of the one-loop Schwinger-Dyson equation for the quark self-energy, in place of $F^2(\vec{p})$ in Eq. (4). The only difference is that F^2 depends on the three-momentum whereas the quoted test function depends on the four-momentum and that the two asymptotic behaviors are different [$\sim 1/p^2$ in the test function of Ref. [14] and $\sim 1/\vec{p}^4$ in F^2

of Eq. (4)]. Otherwise the two effective potentials would be identical. This observation also explains the reason why we have adopted the NJL model instead of *ladder* QCD to generalize the analysis of Ref. [14] at high isospin chemical potentials as the numerical analysis is much simpler in this case.

To fix the free parameters of the model, which are Λ, the average current quarks mass $m=(m_u+m_d)/2$, and the coupling $G=g/\Lambda^2$, we work at zero temperature and quark densities. We first choose the mass scale Λ within the range $\Lambda \sim 500-600$ MeV. Then we determine the strength of the coupling g and the mass parameter m by requiring a light quark condensate of the order $\langle \bar{\Psi}_f \Psi_f \rangle \simeq -(200 \text{ MeV})^3$ and a pion mass $m_\pi \simeq 140$ MeV (the latter evaluated through the curvature of the effective potential in the direction of the pion field and having fixed f_π at its experimental value [36]).

The output parameters are the following:

$$\Lambda = 580 \text{ MeV}; \quad g=7; \quad m=4.5 \text{ MeV}. \tag{6}$$

With these values we obtain a condensate $\langle \bar{\Psi}_f \Psi_f \rangle = -(172 \text{ MeV})^3$ and a constituent quark mass $M_f = 428$ MeV (defined as in Refs. [19,21]). The critical isospin chemical potential at zero temperature turns out to be $\mu_I^C = 89$ MeV. The discrepancy of about 25% (we recall that the expected value of μ_I^C would be $m_\pi/2 \simeq 70$ MeV) is due to the approximate fit procedure. Actually, in our previous work based on *ladder* QCD [14], where f_π was consistently calculated within the model, we got $\mu_I^C = m_\pi/2$.

III. PHASE DIAGRAM FOR CHIRAL SYMMETRY BREAKING AND PION CONDENSATION

In order to discuss the structure of the phase diagram, it is worth summarizing the symmetries of the Lagrangian density in Eq. (1). Both $\mathcal{L}_0$ and $\mathcal{L}_{int}$ are $\mathrm{SU}_L(2) \otimes \mathrm{SU}_R(2) \otimes \mathrm{U}_V^B(1) \otimes \mathrm{U}_A^B(1)$ invariant. The symmetry is reduced by the mass term $\mathcal{L}_m$ to $\mathrm{SU}_V(2) \otimes \mathrm{U}_V^B(1)$ and further reduced from the term $\mathcal{L}_\mu$ which selects a direction in the isospin space, as is evident from Eq. (2), unless $\mu_u = \mu_d$ and thus $\mu_I = 0$. The remaining symmetry can be expressed either as $\mathrm{U}_V^u(1) \otimes \mathrm{U}_V^d(1)$ or $\mathrm{U}_V^B(1) \otimes \mathrm{U}_V^I(1)$, depending on the basis of the fields that we are choosing.

The baryon number symmetry $\mathrm{U}_V^B(1)$ is dynamically respected, whereas a nonvanishing vacuum expectation value of the ρ field defined in Eq. (5) may appear, which dynamically breaks $\mathrm{U}_V^I(1)$. This implies the appearance of a Goldstone mode, which is either the charged π^+ or π^- at the threshold, depending on the sign of μ_I, whereas the other two pions are massive modes.

As far as the scalar condensates χ_u, χ_d [see Eq. (5)] are concerned, they do not break any symmetry. However, since the mass term is small, their value is almost entirely due to the approximate spontaneous breaking of chiral symmetry. Consequently we distinguish regions where the dynamical effect is relevant, from regions where the scalar condensates are of order $\sim m/\Lambda$, namely, where only the effect of the explicit breaking of chiral symmetry survives.

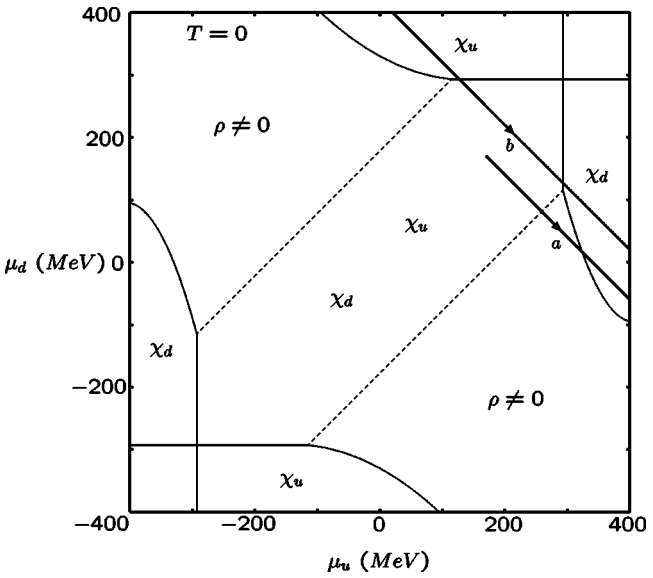

FIG. 1. Phase diagram for chiral symmetry restoration in the plane (μ_u, μ_d) of quark chemical potentials, at $T=0$. Different regions are specified by the nonvanishing of a given condensate, whereas the others are vanishing (ρ) or order $\sim m/\Lambda$ (χ_u and χ_d). Dashed lines are for the continuous vanishing of ρ or for crossover phase transitions for χ_u or χ_d, whereas solid lines are for discontinuous behaviors. The solid lines *a* and *b* refer to specific paths at fixed values of μ_B, with $\mu_B = 170$ MeV (line *a*) relative to Fig. 3 and $\mu_B = 210$ MeV (line *b*) relative to Fig. 4.

The determination of the various phases has been performed numerically by minimizing the one-loop effective potential. We start by showing the results in the (μ_u, μ_d) plane, for fixed values of the temperature. Different regions are labeled, as in Ref. [11], by the symbol of the field which acquires a nonvanishing vacuum expectation value due to dynamical effects, whereas the other fields are vanishing (ρ), or of the order $\sim m/\Lambda$ (χ_u and/or χ_d).

Solid lines refer to discontinuous transitions and dashed lines to continuous ones. However, we recall that strictly speaking only the lines surrounding regions with a nonvanishing field ρ refer to genuine phase transitions, associated with the breaking and restoration of the $\mathrm{U}_V^I(1)$ symmetry.

A. Zero temperature

In Fig. 1 we show the phase diagram in the (μ_u, μ_d) plane at zero temperature. Let us start from the vacuum at $T=\mu_u=\mu_d=0$, at the center of the picture. Here, in the chiral limit, the pions are the Goldstone bosons associated with the spontaneous breaking of $\mathrm{SU}(2)_L \otimes \mathrm{SU}(2)_R$. We have chosen these variables in order to compare the structure of the phase diagram with that obtained in Ref. [11]. However, if we want to recover known results given in terms of the baryon chemical potential, we have to move from the center along the diagonal at $\mu_u = \mu_d$ and thus at $\mu_I = 0$, and increase the absolute value of μ_B. At $|\mu_u + \mu_d|/2 = |\mu_B| = 293$ MeV we meet the approximate restoration of chiral symmetry due to the sudden jump of the condensates of the two (degenerate) quarks to values of order $\sim m/\Lambda$, which is

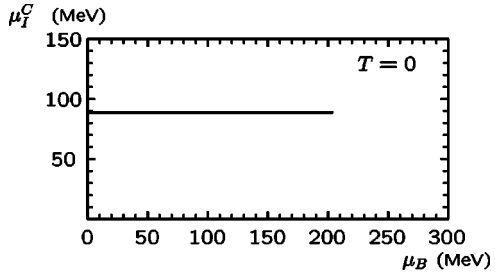

FIG. 2. Critical value of the isospin chemical potential, beyond which a pseudoscalar condensate forms, vs baryon chemical potential, at zero temperature. $\mu_B=204$ MeV is the highest allowed value for pion condensation to occur. The path followed in the phase diagram of Fig. 1 is along the upper half of the dashed line in the lower half plane.

a discontinuous transition. The same thing happens by moving along lines parallel to the main diagonal in the region labeled by χ_u, χ_d, enclosed between the two dashed lines at $|\mu_u-\mu_d|/2=|\mu_I|=89$ MeV (see also Fig. 2 where it is shown that the critical value of μ_I at $T=0$ is independent on μ_B) and by varying $|\mu_B|$. The regions in the top-right and bottom-left corners of Fig. 1 thus have the $U_V^u(1)\otimes U_V^d(1)$ symmetry of $\mathcal{L}$ with $\rho=0$ and χ_u,χ_d of order $\sim m/\Lambda$.

By moving from the center along the diagonal at $\mu_u=-\mu_d$ (and thus $\mu_B=0$) or parallel to it, when crossing one of the two dashed lines at $|\mu_I|=89$ MeV (we have already discussed the origin of the discrepancy between this value and half of the pion mass in the model), the absolute minimum of the effective potential starts to rotate along the ρ direction. We thus have a continuous breaking of $U_V^I(1)$ and a second-order phase transition with one Goldstone mode which is, right along the dashed line, either the π^+ (in the upper part of the diagram) or the π^- (in the lower part). In the chiral limit these two dashed lines merge together in coincidence with the diagonal at $\mu_I=0$ as the pion becomes massless in this limit and the rotation is sudden, giving first-order phase transitions for pion condensation. In this case there are two Goldstone bosons associated with the spontaneous breaking of two U(1) symmetry groups $[U_A^B(1)\otimes U_V^I(1)]$ [25].

Coming back to the massive case, and still with reference to Fig. 1, we conclude that by considering $|\mu_B|$ not too large

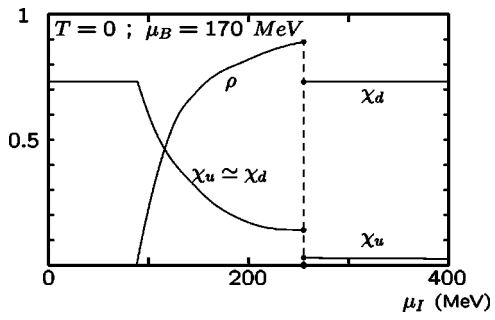

FIG. 3. Scalar and pseudoscalar condensates vs μ_I, for $\mu_B=170$ MeV and $T=0$. The path followed in the phase diagram of Fig. 1 is that of the solid line *a*.

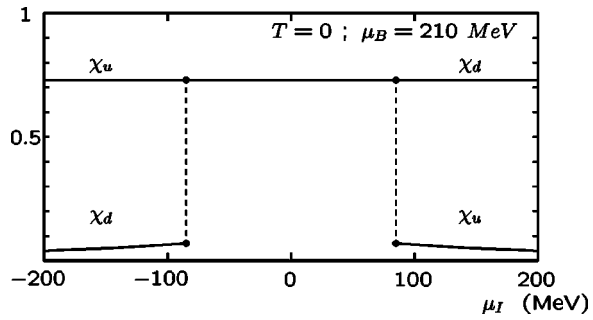

FIG. 4. Scalar condensates vs μ_I for $\mu_B=210$ MeV and $T=0$. The pseudoscalar condensate is zero. The path followed in the phase diagram of Fig. 1 is that of the solid line *b*.

and by growing $|\mu_I|$, we find a second-order phase transition with the rotation of the scalar condensates into the pseudoscalar, namely, we are faced with pion condensation in a relatively simple picture. A difference with Ref. [11] is that we do not find the vanishing of ρ for values of $|\mu_I|$ high with respect to the pion mass, but still sufficiently low to avoid considering superconductive phases (actually, for very low $|\mu_B|$ this transition would occur in the present model for $|\mu_I|\sim 1$ GeV).

To explore the possibility of multiple phase transitions and thus of a richer phenomenology, we need to grow $|\mu_B|$ as, for instance, we do in the case described in Fig. 3 where we follow the path of the solid line *a* in Fig. 1 at $\mu_B=170$ MeV for growing $\mu_I\geqslant 0$. The fields χ_u and χ_d are almost degenerate, both in the region of the approximate dynamical breaking of chiral symmetry (below $\mu_I=89$ MeV) and in the region of spontaneous breaking of $U_V^I(1)$, where they rotate into the ρ field. Then, when the line *a* in Fig. 1 crosses the solid line surrounding the region labeled by χ_d, we see that ρ suddenly jumps to zero with the restoration of the $U_V^I(1)$ group and that χ_u and χ_d split. Actually the latter suddenly acquires a value due to the dynamical breaking of chiral symmetry whereas χ_u undergoes a further decrease and remains of order $\sim m/\Lambda$.

In Fig. 4 we plot the behavior of the scalar condensates χ_u and χ_d vs μ_I at $\mu_B=210$ MeV, namely, by following the

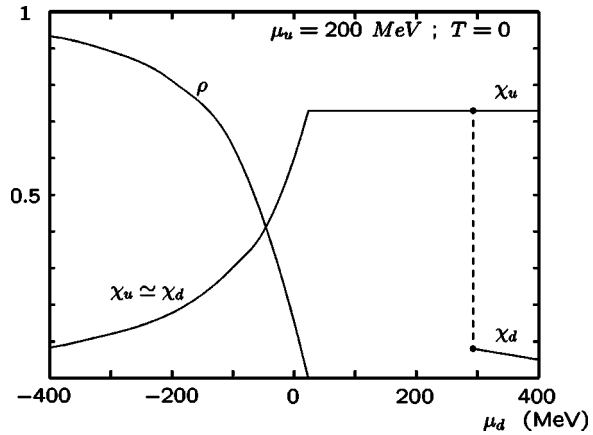

FIG. 5. Scalar and pseudoscalar condensates vs μ_d, for $\mu_u=200$ MeV, $T=0$ (see Fig. 1).

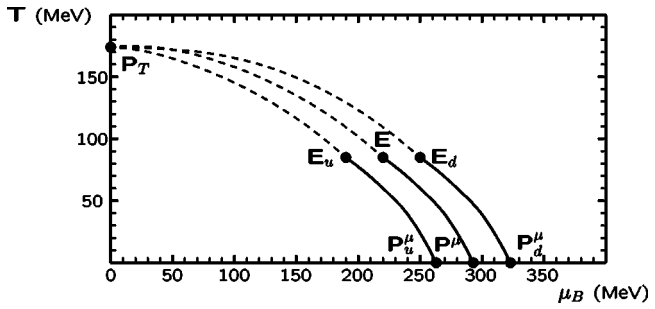

FIG. 6. Phase diagram for chiral symmetry in the (μ_B, T) plane for zero or small isospin chemical potential μ_I. For $\mu_I=0$ (central line), the crossover transition line starts from the point $P_T=(0,174)$ and ends at the point $E=(220,85)$. The line between E and the point $P^\mu=(293,0)$ is the line for the first-order transition with discontinuities in the $\langle\bar{u}u\rangle$ and $\langle\bar{d}d\rangle$ condensates. For $\mu_I=30$ MeV (side lines), the two crossover transition lines start from the point $P_T=(0,174)$ and end at the points $E_u=(190,85)$ and $E_d=(250,85)$. The lines between E_u and the point $P_u^\mu=(263,0)$ and between E_d and the point $P_d^\mu=(323,0)$ are the lines for the first-order transitions with discontinuities in the $\langle\bar{u}u\rangle$ and $\langle\bar{d}d\rangle$ condensates, respectively.

path described by the solid line b in Fig. 1. We see that we never cross the region with $\rho\neq 0$ and that we simply pass from a region where the dynamical effect of the breaking of chiral symmetry is entirely due to a large value of χ_u and χ_d of order $\sim m/\Lambda$ (at large negative μ_I and small μ_u), to a region where this effect manifests itself with a large value of χ_d and χ_u of order $\sim m/\Lambda$ (at large positive μ_I and small

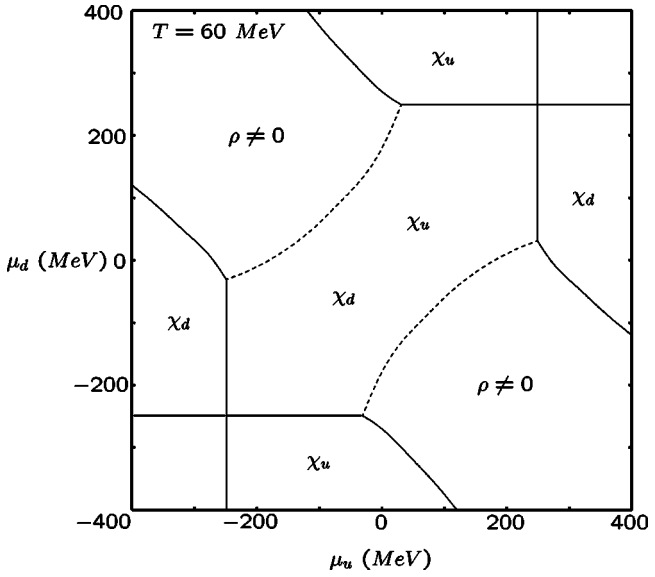

FIG. 7. Phase diagram for chiral symmetry restoration in the plane (μ_u, μ_d) of quark chemical potentials, at $T=60$ MeV, which is below the temperature of the critical ending point (see Fig. 6). Different regions are specified by the nonvanishing of a given condensate, whereas the others are vanishing (ρ) or $\sim m/\Lambda$ (χ_u and χ_d). Dashed lines are lines for the continuous vanishing of ρ or for crossover phase transitions for χ_u or χ_d, whereas solid lines are for discontinuous behaviors.

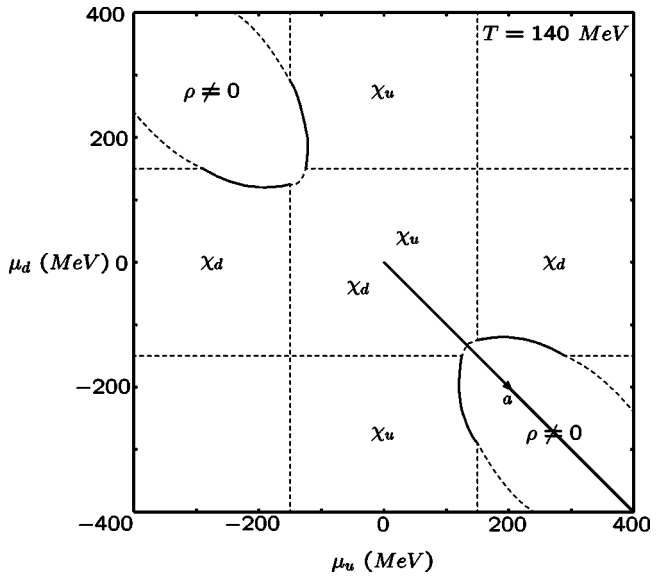

FIG. 8. Phase diagram for chiral symmetry restoration in the plane (μ_u, μ_d) of quark chemical potentials, at $T=140$ MeV, which is above the temperature of the critical ending point (see Fig. 6). Different regions are specified by the nonvanishing of a given condensate, whereas the others are vanishing (ρ) or $\sim m/\Lambda$ (χ_u and χ_d). Dashed lines are lines for the continuous vanishing of ρ or for crossover phase transitions for χ_u or χ_d, whereas solid lines are for discontinuous behaviors. The solid line a refers to the path at $\mu_B=0$ vs $\mu_I\geqslant 0$ followed in Fig. 10.

μ_d). The region in between has almost degenerate and both large χ_u and χ_d. Pion condensation does not occur for this value of μ_B (see also Fig. 2).

Finally, in Fig. 5, we plot the behavior of the condensates at fixed $\mu_u=200$ MeV vs μ_d (see again Fig. 1). The rotation of the pion condensate into the scalar ones occurs when the vertical line at $\mu_u=200$ MeV meets the dashed line at $\mu_I=89$ MeV, which happens for μ_d of few MeV. Then, when μ_d has sufficiently increased, χ_d falls to a small value of

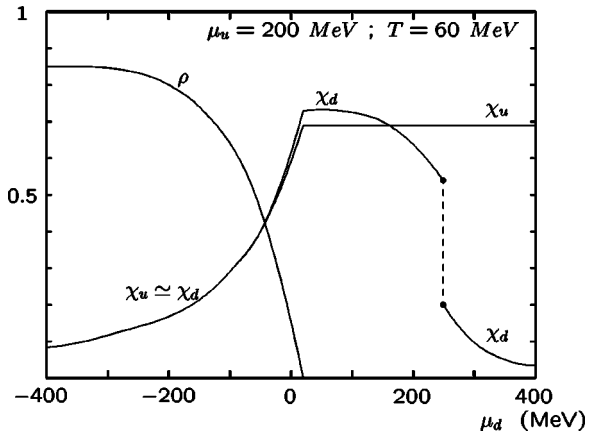

FIG. 9. Scalar and pseudoscalar condensates vs μ_d, for $\mu_u=200$ MeV, $T=60$ MeV (see Fig. 7).

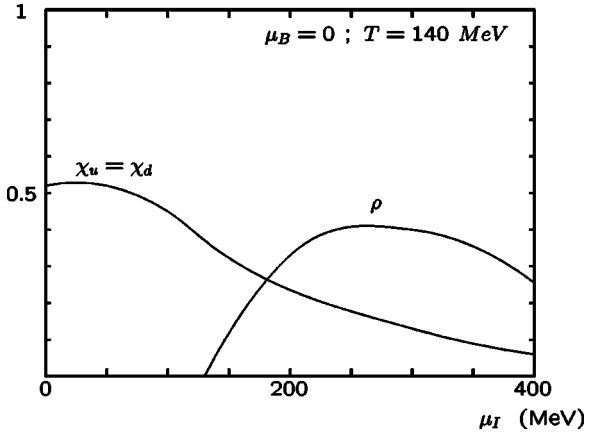

FIG. 10. Scalar and pseudoscalar condensates vs μ_I, for $\mu_B = 0$ and $T = 140$ MeV. The figure is obtained following path a in the phase diagram of Fig. 8.

order $\sim m/\Lambda$ with a discontinuous transition, whereas χ_u remains constant at its large value.

B. Finite temperature

The evolution of the phase diagram for growing temperatures is easily understood as far as the regions with $\rho = 0$ are concerned. Actually, in this case the effective potential at the minimum is the sum of two independent terms, one for each flavor, and the results are straightforwardly given through the analysis of chiral symmetry breaking and restoration for a single flavor at finite temperature and chemical potential (see, for instance, Refs. [16,18]). In Fig. 6 we show the phase diagram at zero, or small isospin chemical potential (see also Refs. [12,14]). From this picture we see that moving along any of the critical lines of chiral symmetry restoration at fixed μ_I, the critical value of the baryon chemical potential μ_B decreases for growing temperatures. Furthermore, for temperatures below that of the critical ending point E, $T < T(E) = 85$ MeV, the transitions are always discontinuous whereas they become crossover transitions for $T > T(E)$. Consequently the regions labeled by χ_u and/or χ_d in Fig. 1 shrink when growing T and their rectilinear sides

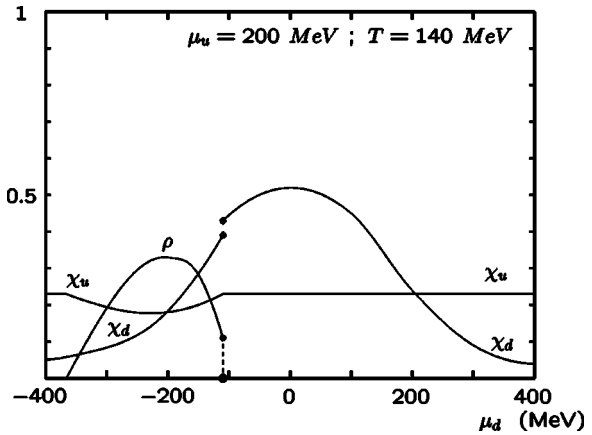

FIG. 11. Scalar and pseudoscalar condensates vs μ_d, for $\mu_u = 200$ MeV, $T = 140$ MeV (see Fig. 8).

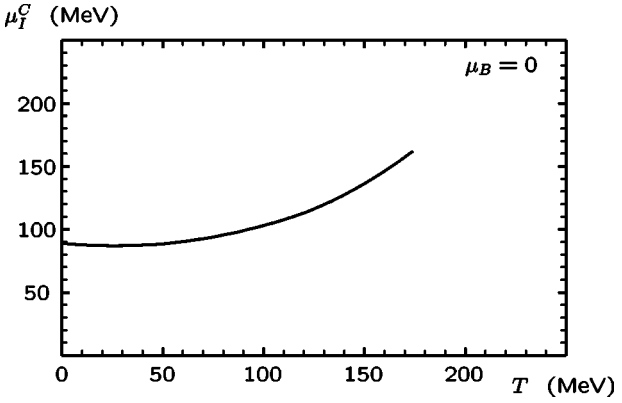

FIG. 12. Critical value of the isospin chemical potential, beyond which a pseudoscalar condensate forms, vs temperature, at zero baryon chemical potential.

become lines of crossover transitions for $T > T(E)$ [see Fig. 1 and Figs. 7 and 8 where we plot the phase diagrams in the (μ_u, μ_d) plane at $T = 60$ MeV and $T = 140$ MeV, which is, respectively, below and above $T(E)$]. The new feature concerns the regions with $\rho \neq 0$, which also reduce their size for growing T, whereas the order of the transitions starts to change from first to second, beginning from the critical points at highest $|\mu_I|$, until they reach the points of the boundaries which coincide with those of the regions labeled by χ_u or χ_d (see Fig. 8). Also the length of the curves of second-order phase transitions to pion condensation at fixed values of $|\mu_B|$ sensibly reduces from low temperatures to high temperatures (see again Fig. 1, and Figs. 7 and 8). A similar behavior, for high T, is found in Ref. [11]. For $T > T(P_T) = 174$ MeV, which is the crossover temperature at zero chemical potential (see Fig. 6), all these regions disappear from the phase diagram, which is thus characterized by $\rho = 0$ and $\chi_u, \chi_d \sim m/\Lambda$.

The behavior of the scalar and pseudoscalar condensates at $T = 60$ MeV are much similar to those at $T = 0$. As an example we plot, in Fig. 9, the condensates at $\mu_u = 200$ MeV and $T = 60$ MeV vs μ_d (compare with Fig. 5). The situation is different if we consider temperatures above $T(E) = 85$ MeV. For instance, at $T = 140$ MeV, we see from Fig. 8, that the structure of the phase diagram is only slightly modified with respect to the case of two independent flavors which undergo crossover phase transitions at sufficiently

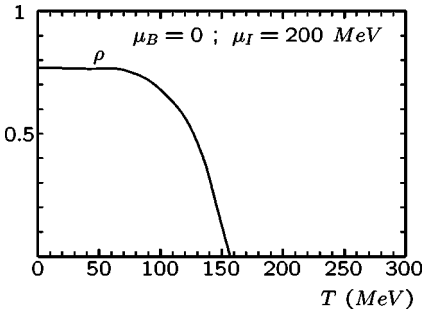

FIG. 13. Pion condensates vs T, for $\mu_B = 0$ and $\mu_I = 200$ MeV. The scalar condensates χ_u and χ_d are of order $\sim m/\Lambda$.

high values of their own chemical potentials (actually the region of pion condensation has sensibly reduced with respect to Figs. 1 and 7). The phase transition associated with the spontaneous breaking of $U_V^I(1)$ can be both second or first order, depending on the path followed. In Fig. 8, the solid line *a* refers to a path at $\mu_B=0$ vs $\mu_I \geqslant 0$ where the transition to pion condensation is continuous. The behavior of the condensates relative to this path is plotted in Fig. 10. In Fig. 11 we plot the scalar and pseudoscalar condensates at $\mu_u=200$ MeV and $T=140$ MeV vs μ_d.

In Fig. 12 we plot the value of the critical isospin chemical potential μ_I^C beyond which a pion condensate forms vs temperature T at zero baryon chemical potential μ_B. The growth of μ_I^C is easily understood since the pion mass (which should be twice μ_I^C) is expected to grow near the critical temperature for chiral symmetry restoration [38]. On the other hand, no phase transition to pion condensation is expected above the crossover temperature for chiral symmetry restoration. Thus the line of critical values ends at $T=174$ MeV.

The pion condensate is also expected to decrease for growing temperatures: in Fig. 13 we show ρ vs T at $\mu_B=0$ and $\mu_I=200$ MeV. Similar behaviors are obtained for fixed values of μ_B and μ_I.

IV. CONCLUSIONS

In this paper we have continued the study of pion condensation at finite baryon and isospin density in the NJL model that we started in Ref. [14] in the case of *ladder* QCD for small isospin chemical potentials. The extension to higher isospin chemical potentials confirms the structure predicted in Ref. [11], where two-flavor QCD was simulated in the context of a random matrix model. Some difference between the two analyses is present, at low temperatures, in the region of high isospin chemical potentials, at the boundary of the region where color superconductivity should take place. Actually in this region we find that pion condensation is still active, whereas in Ref. [11] the authors find that the pion condensate vanishes. We have also shown the expected behavior of scalar and pion condensates by following different paths, for growing temperatures, both in the plane of quark chemical potentials (μ_u,μ_d) and in that of isospin and baryon chemical potentials (μ_I,μ_B). The analysis that we have performed should also be confirmed, with only small quantitative differences, within *ladder* QCD.

[1] M. Buballa and M. Oertel, Phys. Lett. B **457**, 261 (1999).
[2] P.F. Bedaque, Nucl. Phys. **A697**, 569 (2002).
[3] D. Toublan and J.J.M. Verbaarschot, Int. J. Mod. Phys. B **15**, 1404 (2001).
[4] A. Steiner, M. Prakash, and J.M. Lattimer, Phys. Lett. B **486**, 239 (2000).
[5] D.T. Son and M.A. Stephanov, Phys. Rev. Lett. **86**, 592 (2001).
[6] M.G. Alford, J.A. Bowers, and K. Rajagopal, Phys. Rev. D **63**, 074016 (2001).
[7] K. Splittorff, D.T. Son, and M.A. Stephanov, Phys. Rev. D **64**, 016003 (2001).
[8] J.B. Kogut and D. Toublan, Phys. Rev. D **64**, 034007 (2001).
[9] A.W. Steiner, S. Reddy, and M. Prakash, Phys. Rev. D **66**, 094007 (2002).
[10] F. Neumann, M. Buballa, and M. Oertel, Nucl. Phys. **A714**, 481 (2003).
[11] B. Klein, D. Toublan, and J.J.M. Verbaarschot, Phys. Rev. D **68**, 014009 (2003).
[12] D. Toublan and J.B. Kogut, Phys. Lett. B **564**, 212 (2003).
[13] M. Frank, M. Buballa, and M. Oertel, Phys. Lett. B **562**, 221 (2003).
[14] A. Barducci, G. Pettini, L. Ravagli, and R. Casalbuoni, Phys. Lett. B **564**, 217 (2003).
[15] A. Barducci, R. Casalbuoni, S. De Curtis, R. Gatto, and G. Pettini, Phys. Lett. B **231**, 463 (1989).
[16] A. Barducci, R. Casalbuoni, S. De Curtis, R. Gatto, and G. Pettini, Phys. Rev. D **41**, 1610 (1990).
[17] S.P. Klevansky, Rev. Mod. Phys. **64**, 649 (1992).
[18] A. Barducci, R. Casalbuoni, G. Pettini, and R. Gatto, Phys. Rev. D **49**, 426 (1994).
[19] T. Hatsuda and T. Kunihiro, Phys. Rep. **247**, 221 (1994).
[20] M.A. Halasz, A.D. Jackson, R.E. Shrock, M.A. Stephanov, and J.J.M. Verbaarschot, Phys. Rev. D **58**, 096007 (1998).
[21] J. Berges and K. Rajagopal, Nucl. Phys. **B538**, 215 (1999).
[22] K. Rajagopal and F. Wilczek, in *At the Frontier of Physics: Handbook of QCD*, edited by M. Shifman (World Scientific, Singapore, in press), Vol. 3, p. 2061.
[23] A. Jakovac, A. Patkos, Z. Szep, and P. Szepfalusy, Phys. Lett. B **582**, 179 (2004).
[24] J.B. Kogut and D.K. Sinclair, Phys. Rev. D **66**, 014508 (2002).
[25] J.B. Kogut and D.K. Sinclair, Phys. Rev. D **66**, 034505 (2002).
[26] S. Gupta, hep-lat/0202005.
[27] P. de Forcrand and O. Philipsen, Nucl. Phys. **B642**, 290 (2002).
[28] D.K. Sinclair, J.B. Kogut, and D. Toublan, hep-lat/0311019.
[29] Z. Fodor and S.D. Katz, Phys. Lett. B **534**, 87 (2002).
[30] Z. Fodor and S.D. Katz, J. High Energy Phys. **03**, 014 (2002).
[31] C.R. Allton *et al.*, Phys. Rev. D **66**, 074507 (2002).
[32] M. D'Elia and M.P. Lombardo, Phys. Rev. D **67**, 014505 (2003).
[33] Y. Nishida, Phys. Rev. D **69**, 094501 (2004).
[34] S. Hands and D.N. Walters, Phys. Rev. D **69**, 076011 (2004).
[35] M.G. Alford, K. Rajagopal, and F. Wilczek, Phys. Lett. B **422**, 247 (1998).
[36] A. Barducci, R. Casalbuoni, S. De Curtis, D. Dominici, and R. Gatto, Phys. Rev. D **38**, 238 (1988).
[37] M.G. Alford, J.A. Bowers, J.M. Cheyne, and G.A. Cowan, Phys. Rev. D **67**, 054018 (2003).
[38] A. Barducci, R. Casalbuoni, S. De Curtis, R. Gatto, and G. Pettini, Phys. Rev. D **46**, 2203 (1992).